Sensors and Actuators A 295 (2019) 653–662

Contents lists available at ScienceDirect

Sensors and Actuators A: Physical

journal homepage: www.elsevier.com/locate/sna

Using complex multi-dimensional vibration trajectories in ultrasonic bonding and welding

Reinhard Schemmel[a,*], Tobias Hemsel[a], Collin Dymel[a], Matthias Hunstig[b], Michael Brökelmann[b], Walter Sextro[a]

[a] Paderborn University, Warburger Str. 100, 33098 Paderborn, Germany
[b] Hesse GmbH, Lise-Meitner-Straße 5, 33104 Paderborn, Germany

ARTICLE INFO

Article history:
Received 21 December 2018
Received in revised form 11 April 2019
Accepted 19 April 2019
Available online 21 June 2019

Keywords:
Ultrasonic bonding
Ultrasonic welding
Multi-dimensional bonding
Complex vibration
Multi-frequent
Two-dimensional friction model

ABSTRACT

Ultrasonic joining is a common industrial process. In the electronics industry it is used to form electrical connections, including those of dissimilar materials. Multiple influencing factors in ultrasonic joining are known and extensively investigated; process parameters like ultrasonic power, bond force, and bonding frequency of the ultrasonic vibration are known to have a high impact on a reliable joining process and need to be adapted for each new application with different geometry or materials. This contribution is focused on increasing ultrasonic power transmitted to the interface and keeping mechanical stresses during ultrasonic bonding low by using a multi-dimensional ultrasonic transducer concept. Bonding results for a new designed connector pin in IGBT-modules achieved by multi- and one-dimensional bonding are discussed.

1. Introduction

Since about 1954 an abrupt change of the joining technique in microelectronics occurred when the mesa transistor was developed which lead to a significantly decreased size of the contact areas and new joining processes were developed to create reliable electrical connections; in 1960 Sonobond received the first patent for ultrasonic metal welding, [1]. The ultrasonic joining technique was then further developed and is used in various applications these days. Ultrasonic bonding is a solid-state joining process, where the induced oscillating shear between the faying surfaces is mainly responsible for the metallurgical bond formation. During bond formation, different processes take place, thus the bond process is typically divided into different phases, [2,3], see Fig. 1.

In the first phase (Pre-Deformation Phase) a static touchdown force F_{TD} is applied to the workpiece. The workpiece is clamped by the bond tool (wedge) at the bond position and an initial contact area is created, [4].

In the next phase (Cleaning Phase), the ultrasonic vibration x_W and the bond normal force F_{bn}, which can differ from F_{TD}, are applied to the workpiece. When the induced oscillating shear forces are large enough to overcome the sticking-force between the workpiece and substrate, sliding occurs. The oxide layers and other contaminations are then detached from the faying surfaces and are transported to the peripheral contact region, [5,6].

In the third phase (Deformation Phase), high plastic deformation of the workpiece and the interface region of the substrate can be seen, even though the normal force F_{bn} is not increased significantly; the effect of high deformation under influence of ultrasonic vibration is known as the Ultrasonic Softening Effect, [7]. During the Deformation Phase, the contact roughness is reduced and thus the real contact area is increased; the reduction of the gap between the two faying surfaces is crucial for the intermetallic bond formation, [8]. Additionally first micro-junctions occur in areas, where contact asperities are plastically deformed, [9].

In the last phase (Interdiffusion Phase), material flow between workpiece and substrate can be seen. The material flow occurs without melting the materials and is induced by the oscillating shear stress and plastic strain in the interface, [10]. The material flow leads to an intermetallic connection between workpiece and substrate; the two metals are not molten, thus dissimilar metals with different melting temperatures can be bonded, [11–13].

Depending on the application and the workpieces that can vary in contact area size and material, ultrasonic joining is divided into fine and heavy wire bonding, ribbon bonding, and ultrasonic welding, Table 1. Fine wire bonding is used for low-current connec-

* Corresponding author.
E-mail address: reinhard.schemmel@upb.de (R. Schemmel).

https://doi.org/10.1016/j.sna.2019.04.025
0924-4247/

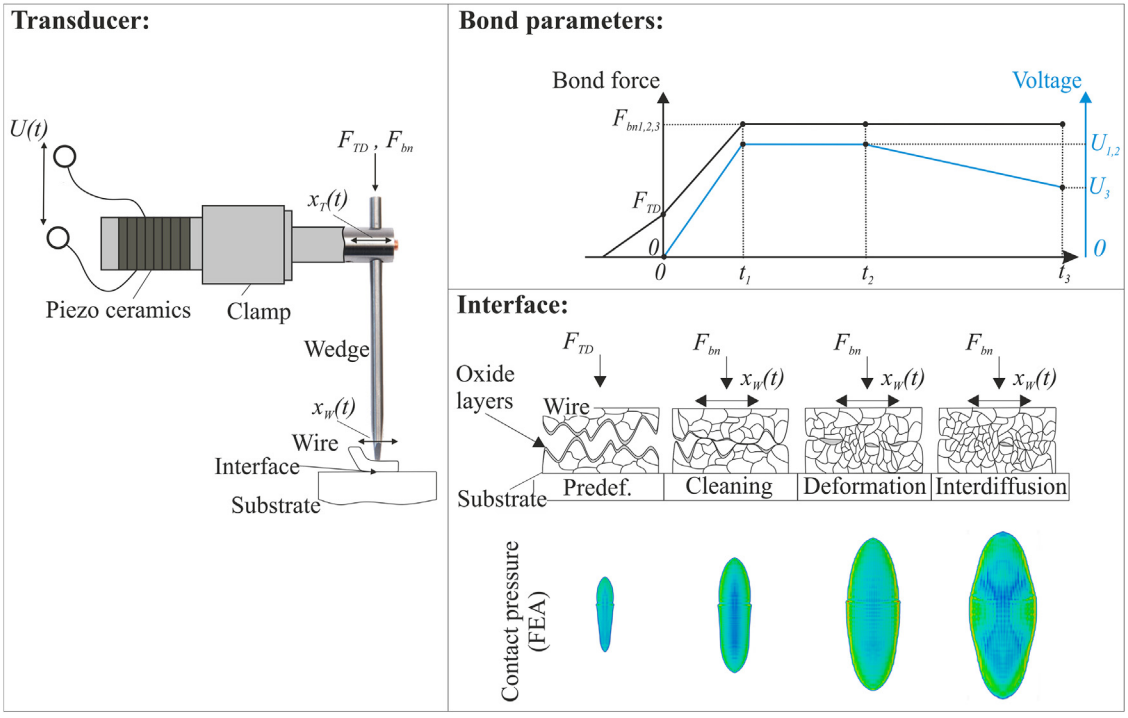

Fig. 1. Left: Ultrasonic transducer for wire bonding, driven by the oscillating voltage $U(t)$ and the wedge, clamping the wire by the bond normal force F_{bn}. The wedge is excited to a bending oscillation by the transducer amplitude $x_T(t)$ and the wire is excited by the wedge amplitude $x_W(t)$. **Right:** Trajectories of the main bondparameters (bondforce F_{bn}, and voltage $U(t)$) over the bond duration and the changing interface conditions during the four bond phases. During the bond formation, the contact area increases and the contact pressure distribution changes, which can be seen in Finite Element Analysis (FEA) results.

Table 1
Comparison of the different process technologies in ultrasonic joining by the size of the workpiece, typical workpiece materials, and equipment used in ultrasonic bonding and welding. For wires the diameter, for ribbons and stranded wires the cross section of the workpieces are given. For metal spot welding the welded contact and the sheet thickness are given.

Technology	Size	Typical material	Equipment (power/frequency)
Fine wire bonding (wedge-wedge)	Diameter 12.5–75 µm	AlSi1, AlMg, Au, Ag, Cu, Pt	Bonding machine (2W/60–140 kHz) with fine wire/ribbon bond head
Fine ribbon bonding	Cross section 6 × 35–25 × 250 µm²		
Heavy wire bonding	Diameter 50–600 µm	Al, Cu, Al-clad Cu	Bonding machine (50–200 W/40–100 kHz) with heavy wire/ribbon bond head
Heavy ribbon bonding	Cross section 25 × 250–400 × 2000 µm²		
Ultrasonic metal spot welding	Contact area 0.3–100 mm², Sheet thickness up to 5 mm	Cu, CuFe2P, CuSn6, CuNiSi	Welding press (0.5–10 kW/20–40 kHz)
Ultrasonic welding of stranded wires	Cross section 0.26–60 mm²	Cu	

tions in devices like lead-frame packages, small sensors or antenna designs for CMOS wafers where the antenna is designed by the loop of the wire bond, [14,15]. In high frequency applications fine ribbon bonding is used to reduce the cross section and thereby the self induction of the workpiece at high switching frequencies (skin effect), [16]. In heavy wire bonding, larger wire diameters compared to fine wire bonding are used to connect electrical devices like insulated-gate bipolar transistors (IGBT) in high power applications, such as high power inverters which are used in wind turbines, electrical vehicles or solar modules. To further increase the contacting area and the efficiency of the electronic devices in high power applications, heavy ribbon bonding is used, [17,18].

Compared to wire and ribbon bonding, ultrasonic welding is performed at about 10-times higher ultrasonic power and bond normal force F_{bn}. Applications of ultrasonic welding are the joining of dissimilar materials in lightweight constructions in automobile industry (e.g. Al-steel, Al-Mg), joining large electrical connections like multi-strand aluminum cables for battery harnesses in automobiles, and welding copper terminals in IGBT-modules, [12,19,20]. Welding dissimilar materials like Al-Cu sheets under high bond normal force and high ultrasonic power leads to massive deformation in the interface which can be seen in swirls and voids in optical images of the cross section in the interface and the interface temperature rises up to 280 °C, [12,21,22]. When joining workpieces with large contacting area, increasing the ultrasonic power and the bond normal force is unavoidable, leading to larger dynamical stresses in the interface. When welding e.g. Al-Cu sheets, the high deformation and dynamical stresses during welding can be tolerated, since no surrounding parts can be damaged. In electronic applications like welding terminals in IGBT-modules, those dynamical stresses during the welding process can lead to failure of the pre-assambed package; e.g. already bonded wires connecting the chips in IGBT-modules can be damaged, delamination of the substrate can occur, and voids in the metallic interface can arise; with these failure modes, the lifetime of the electrical interconnections is decreased. The main goal when welding large workpieces

in electronic applications is to decrease the dynamical mechanical stress in the interface during the welding process for increasing the reliability of the product.

On the other hand, in high power applications, a trend of steadily increasing the transmittable electrical power and reducing the size of the electronic parts for lightweight can be seen, [23]. As a result, new challenges in high power applications are the rising demands on the electrical connection with larger junction temperatures and higher mechanical stresses in the bond connections. Electrical parts like LED modules, main inverters, on-board chargers, DC/DC converters, the battery management system or the engine control unit are parts in automobiles, which are highly stressed by temperature changes and harsh vibration levels in new generation automobiles, [24]. The connections are tested by the testing procedure described in AEC-Q100 and Q101, [25]; e.g. the grade 1 standard defines 1000 cycles in the range −55 °C/+150 °C. Especially solder joints fail under these harsh test conditions and new solder alloys need to be developed. Ultrasonically bonded connections on the other hand - with higher mechanical strength of the intermetallic bond connection - show higher reliability under these conditions. Thus substitution of solder joints by ultrasonically bonded connections can increase the reliability of electrical devices in future.

In this contribution, the impact of the multi-dimensional vibration parameters like the bonding frequency and the shapes of the different vibration loci on the bond formation are summarized in the current state of science. A multi-dimensional ultrasonic transducer concept with mono- and multi-frequent planar oscillation loci and its control concept is presented. For validation of the multi-dimensional transducer, vibration trajectories of the ultrasonic bonding tool under loaded conditions during ultrasonic bonding are shown. For a profound understanding of the impact of the planar multi-frequent vibration trajectories on the bond formation, simulation results of a parameter sweep with a two-dimensional friction model are analyzed. In addition to the numerical investigations, bonding experiments for a new connector pin design for IGBT modules are utilized to evaluate the bond quality for one- and two-dimensional ultrasonic bonding.

2. Impact of the bonding frequency and direction

2.1. Background: bonding frequency

In the past, several approaches for investigating the impact of different bonding frequencies have been reported, [26]– [32]. Onuki et al. reported in [27] that bonding aluminum wires with 500μm diameter on 5μm thick AlSi films on transistor chips with 110 kHz raises the bond strength and decreases the deformation of the Al-wire compared to 60 kHz. Chan et al. found in [28] for bonding Au-wires with 25.4 μm diameter on a PCB bond pad with two bonding frequencies at 62 kHz and 138 kHz that bonding with 138 kHz leads to a larger bond process window (bond pad temperature and ultrasonic power). In contrast to the results in [28], Charles et al. reported in [29] and [30] for bonding Au-wire with 25.4 μm diameter, bonding frequencies of 60 kHz and 100 kHz, three different substrate metallizations, and three different test patterns that the benefits of the different bonding frequencies were dependent on the metallization and a larger process window for 60 kHz compared to 100 kHz was observed.

Heinen et al. reported in [31] for bonding on integrated circuits (ICs) with assembled test chips on a polymeric dielectric that bonding with a frequency twice as high than 60 kHz provides additional process reliability and a larger process window. The high bonding frequencies provided more focused ultrasonic energy that does not penetrate as deeply into the chip and on pads on soft polymers such as Teflon or unreinforced polyimide the bonding quality is improved with higher frequency.

Schemmel et al. reported in [32] for bonding on substrate substructures with resonance frequencies near the bonding frequency of the transducer, that a higher bonding frequency than the resonance frequency of the substructure is beneficial to reduce substrate vibration amplitudes during the bond process. This effect was explained by the absorbing character of mechanical systems when being excited with frequencies higher than their resonance frequency.

2.2. Background: Multi-dimensional bonding

In ultrasonic joining, one-dimensional translatory motion welding systems are most established. As an alternative welding system, multi-dimensional ultrasonic bonding has been investigated by several different researchers, [33]-[41]. Asami et al. reported in [34] that the one-dimensional translatory motion of the transducer leads to directional bond quality characteristics of the contact area. Contradictory, Hetrick et al. reported in [35] that no directionality was found for ultrasonic welding with a one-dimensional ultrasonic welding system.

Asami et al. presented in [36] a multi-dimensional vibration system with a one-dimensional translatory vibration and additional torsional movement of the transducer-horn; bonding experiments showed that a multi-dimensional vibration locus increases the weld quality significantly compared to the one-dimensional welding process at the same electric input power. Multi-frequency bonding tests with two-dimensional vibration locus at 18.3 kHz and 29.3 kHz were performed in welding dissimilar metals (Al and Cu plates) by Asami et al. and Tamada et al. in [37–39]. It was found, that using a non-directional vibration locus (ratio between the two vibration amplitudes 1:1) produced the highest weld strength.

Dymel et al. presented a versatile test rig for multi-dimensional ultrasonic bonding of connector pins of a semiconductor module in [40]. The shear force values were evaluated depending on the ratio of the two vibration amplitudes; by increasing the ratio to one (circle locus) the shear force value was increased by a factor of 3.22 compared to one-dimensional bonding. Dymel et al. also reported in [41], that a circular ultrasonic excitation of the rotationally symmetrical connector pin can lead to a rotation of the pin itself.

3. Multidimensional transducer concept

The concept of the multi-dimensional ultrasonic transducer is shown in Fig. 2. Four single transducers are mounted to a coupling element in the center and are oriented perpendicular to each other. In the center of the coupling element the ultrasonic bonding tool is mounted. The pairs of transducers opposing each other are moving in the same direction and are called “channels” in the following; the channels are operated by excitation voltages $U_1(t)$ and $U_2(t)$. Different kinds of multi-dimensional vibration loci can be excited with this transducer concept; e.g. when both channels are operated at the same bonding frequency an elliptical locus at the tool is achieved. When the two channels are equipped with transducers with different bonding frequencies, multi-frequent complex planar vibration loci can be generated at the tool tip.

The ultrasonic transducer is made of lead zirconate titanate (PZT) for the piezo ceramics and stainless steel for the other parts of the transducers including the coupling element. The ultrasonic bonding tool is made of hardened stainless steel with a Rockwell hardness of approx. 48 HRC to achieve high reliability of the bonding tool.

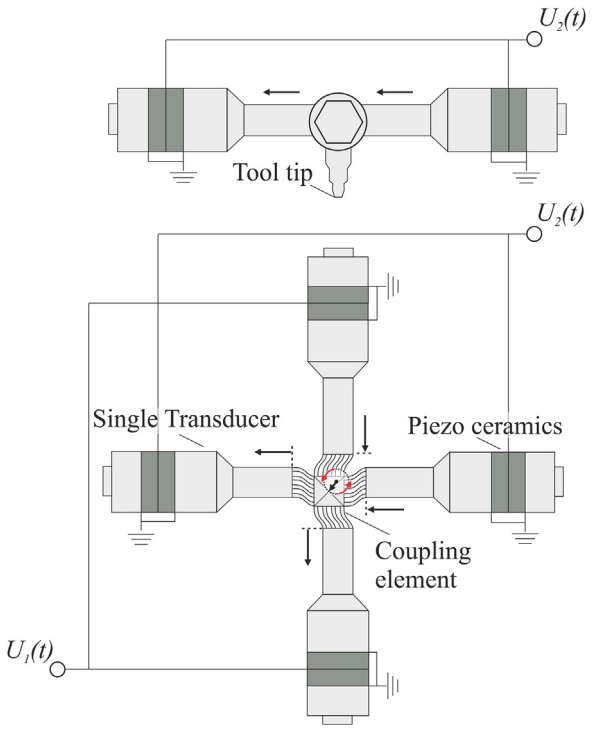

Fig. 2. Concept of the multi-dimensional transducer. Four single transducers are mounted to a coupling element in the center and are excited by voltages U_1 and U_2, so that opposing pairs of transducers move in the same direction.

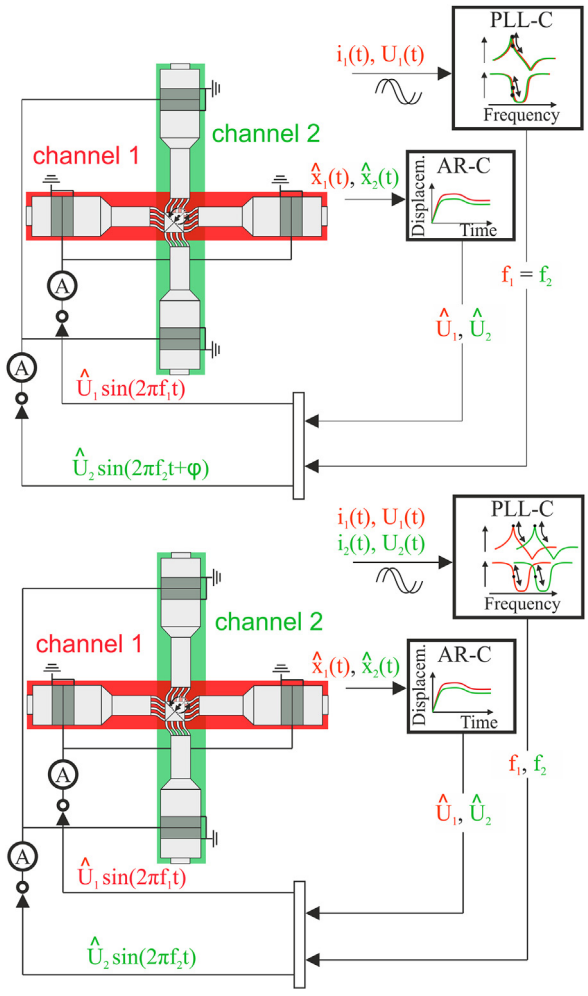

Fig. 3. Control system for the multi-dimensional transducer for the circle mode on top and the rectangle mode at the bottom; a PLL-controller is used to control the phase between current and voltage. In case of the circle mode, only the phase of channel 1 is controlled and the frequency f_1 is applied to channel 2. For the rectangle mode, both channels are operated independent from each other. The AR-controller controls the ratio between the displacement amplitudes of both channels. Only for the circle mode, the phase φ of the oscillating voltage $\hat{U}_2 \sin(2\pi f_2 + \varphi)$ of channel 2 is adjusted.

In Fig. 3 the control concept for an elliptical mono-frequent "circle mode" (top) and a multi-frequent "rectangle mode" (bottom) are shown. In case of the circle mode, the frequency of channel 1 is operated by a Phase Locked Loop controller (PLL-C) which controls the phase difference between voltage and current. Typically, in case of one-dimensional transducers, the PLL controller is set to control the frequency to the resonance frequency (phase 0°) of the transducer; in case of the multi-dimensional transducer and the circle mode, the PLL controller is set to drive both channels in an efficient common operating point which may differ from the resonance frequencies of the channels, depending on the mistuning of the resonance frequencies between both channels. The second controller is an Amplitude Ratio controller (AR-C) to control the ratio between the displacement amplitudes $\hat{x}_1$ and $\hat{x}_2$ of the two channels; the displacement is observed from laser vibrometer measurements directly at the tool tip and by controlling the ratio between the oscillation amplitudes $\hat{x}_1$ and $\hat{x}_2$ to one, a circular locus at the tool tip can be achieved. For this, the phase shift φ of the oscillating voltage $\hat{U}_2 \sin(2\pi f_2 t + \varphi)$ of channel 2 is adjusted.

In case of the rectangle mode, the resonance frequencies of the two channels are significantly different from each other (e.g. $|f_1 - f_2|$ »1 kHz). Both channels are operated in their own resonance frequency by the PLL controller, so both channels are operated with different bonding frequencies f_1 and f_2. The AR-controller is used to control the ratio between the displacement amplitudes $\hat{x}_1$ and $\hat{x}_2$. The multi-dimensional transducer was operated in both modes - the mono-frequent circle mode and the multi-frequent rectangle mode - under loaded conditions during ultrasonic bonding, Fig. 4. The figures show the vibration loci, measured by a Polytec CLV 3D laser vibrometer at the tool tip. For the circle mode, the two channels are operated close to the resonance frequency of both channels at approx. 20 kHz. The amplitude ratio for the AR-controller is 1, leading to an elliptical vibration very close to a circular locus. A stable planar vibration locus is achieved by the controllers after a few oscillation cycles. For the rectangle mode, channel 1 was operated at its resonance frequency at approx. 55 kHz and channel 2 at approx. 20 kHz. The amplitude ratio between both channels was set to 0.4. Since there is no fix phase difference between two harmonic signals of different frequencies, the vibration of the multi-frequent vibration locus fills a rectangle of the width of $\hat{x}_1$ and the length of $\hat{x}_2$ during the bond formation.

4. Numerical investigations on the impact of vibration trajectories

Frictional processes in the interface between workpiece and substrate play an important role for the bond formation in the cleaning and deformation phases. Increasing the frictional power in the interface efficiently without increasing the mechanical stress significantly is the main goal to prevent damage of the substrate. In the following, a generalized point contact model for one- and two-dimensional excitation trajectories for numerical investigations on the impact of the vibration loci on the frictional power is presented, which has been published in [42], and [43], Fig. 5.

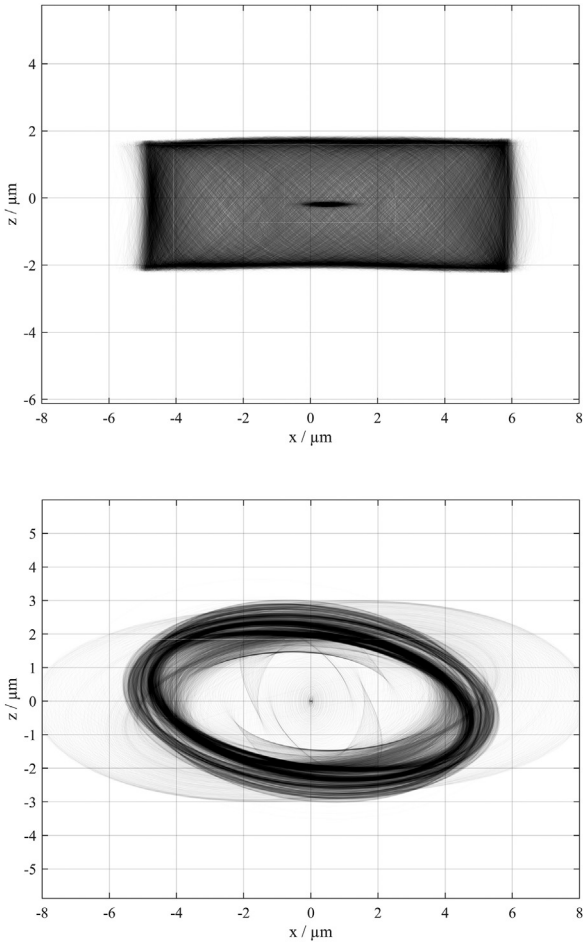

Fig. 4. Measurement of the vibration locus at the tool tip by a 3D laser vibrometer during ultrasonic bonding with the rectangle mode at approx. 20 kHz and approx. 55 kHz (top) and the circle mode (bottom) at approx. 20 kHz over a bond duration of 200 ms; the lines are plotted with transparency for the whole bond duration. A amplitude ratio of 0.4 was used for the rectangle mode and of 1 for the circle mode.

The local vectors in the coordinate system P to the projection point W' of the excitation point W, to the contact point S on the substrate, and to the friction force are given by

$$\begin{aligned} \vec{l}_{W'}(t) &= {}_{\mathrm{P}}\begin{bmatrix} x_{W'}(t) \\ y_{W'}(t) \end{bmatrix} \quad ; \quad \vec{l}_S(t) = {}_{\mathrm{P}}\begin{bmatrix} x_S(t) \\ y_S(t) \end{bmatrix} \\ \vec{F}_f(t) &= {}_{\mathrm{P}}\begin{bmatrix} x_f(t) \\ y_f(t) \end{bmatrix}. \end{aligned} \tag{1}$$

The differential equation system during sliding of the contact point vector $\vec{l}_S(t)$ and the friction force vector $\vec{F}_f(t)$ is given by

$$\begin{aligned} \dot{\vec{l}}_S &= \frac{\vec{F}_f^T \dot{\vec{l}}_{W'} - \frac{\mu^2}{c_t} F_n \dot{F}_n}{\vec{F}_f^T \vec{F}_f} \vec{F}_f \\ \dot{\vec{F}}_f &= c_t \left(\dot{\vec{l}}_{W'} - \frac{\vec{F}_f^T \dot{\vec{l}}_{W'} - \frac{\mu^2}{c_t} F_n \dot{F}_n}{\vec{F}_f^T \vec{F}_f} \right) \vec{F}_f. \end{aligned} \tag{2}$$

During the sticking state, the differential equations of the contact point and the friction force are given by

$$\begin{aligned} \dot{\vec{l}}_S &= \vec{0} \\ \dot{\vec{F}}_f &= c_t \dot{\vec{l}}_{W'}. \end{aligned} \tag{3}$$

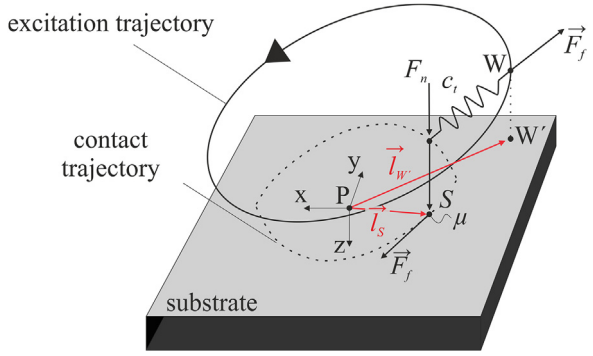

Fig. 5. Two dimensional friction point contact model with the excitation point W, the vertical projection point W' of W, the contact stiffness c_t, the normal force F_n, the friction force F_f, the friction coefficient μ, the origin P of the coordinate system, and the contact point S.

Table 2
Values of the simulation parameters which are varied in a parameter sweep.

Parameter	Description	Values
$\hat{a}_1$	amplitude x-direction	6 µm
$\hat{a}_2$	amplitude y-direction	1, 1.25,... 6 µm
f_1	frequency x-direction	20 kHz
f_2	frequency y-direction	21, 22,... 100 kHz
t	simulation time	4 ms

The transition from slip to stick state occurs, when the condition $\dot{\vec{l}}_S = \vec{0}$ is satisfied. From Eq. (2) follows the transition criterion

$$\vec{F}_f \dot{\vec{l}}_{W'} - \frac{\mu^2}{c_t} F_n \dot{F}_n = 0. \tag{4}$$

For determining the transition from the stick to slip state, the transition function $\Phi(t)$ is used:

$$\Phi = \left\| \vec{F}_f \right\| - \mu F_n. \tag{5}$$

With Eq. (5), the transition from stick to slip can be calculated by

$$\Phi \geq 0 \quad \text{and} \quad \dot{\Phi} > 0. \tag{6}$$

Eqs. (2), and (3) are implemented with the transition criterion in Eqs. (4) and (6) in MATLAB for simulation of the frictional process at different one- and two-dimensional and multi-frequent excitation loci of the point W. The excitation loci have the form of Eq. (7) where $f_1 x$ and f_2 are the bonding frequencies in x- and y-direction in the coordinate system P, $\hat{a}_1$ and $\hat{a}_2$ are the corresponding oscillation amplitudes.

$$\vec{l}_{W'}(t) = {}_{\mathrm{P}}\begin{bmatrix} \hat{a}_1 \sin(2\pi f_1 t) \\ \hat{a}_2 \sin(2\pi f_2 t) \end{bmatrix} \tag{7}$$

For the simulations, the rectangle mode is investigated; the values of the excitation in x-direction are kept constant with the excitation frequency $f_1 = 20$ kHz and the amplitude $\hat{a}_1 = 6$ µm and the parameters in y-direction are changed in the range shown in Table 2. For the simulation time, 4 ms was chosen which leads to 80 oscillation cycles of the 20 kHz vibration; longer simulation duration showed no difference in the simulation results.

There are some special cases of planar vibration loci which vary for $f_1 = 20$ kHz and different frequencies f_2, e.g. $f_2 = 40$ kHz, 45 kHz, and 60 kHz, see Fig. 6. The period length of a two-dimensional vibra-

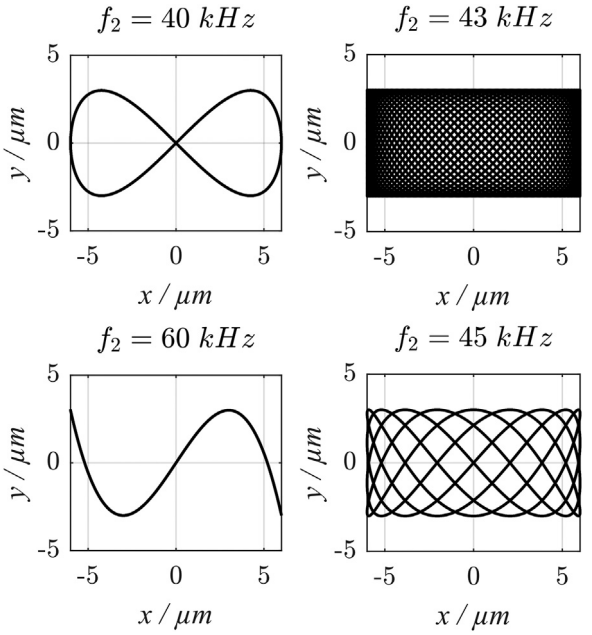

Fig. 6. Planar vibration locus with a constant excitation frequency f_1 = 20 *kHz* and different excitation frequencies f_2. For f_2= 40 kHz, 45 kHz and 60 kHz, a stationary vibration locus is observed. For f_2 = 43 *kHz* a non-stationary vibration locus fills the shape of a rectangle in the vibration plane over the vibration duration.

tion locus can be calculated by the greatest common divisor (gcd) of the two frequencies:

$$\begin{aligned} &\text{gcd}(20\ \text{kHz}, 40\ \text{kHz}) = 20\ \text{kHz} \\ &\text{gcd}(20\ \text{kHz}, 43\ \text{kHz}) = 1\ \text{kHz} \\ &\text{gcd}(20\ \text{kHz}, 45\ \text{kHz}) = 5\ \text{kHz} \\ &\text{gcd}(20\ \text{kHz}, 60\ \text{kHz}) = 20\ \text{kHz} \end{aligned} \tag{8}$$

For excitation frequencies f_2 = 40 kHz and 60 kHz, the superposition of both harmonic signals leads to a periodic vibration locus, with the period length of the 20 kHz vibration. In case of $f_2 = 2\,f1$, $4\,f_2, \ldots$ a circular motion and in case of $f_2 = 3\,f_1, 5\,f_1$ kHz, . . . a motion following a line can be seen.

For f_2 = 43 kHz the period length of an 1 kHz vibration and for f_2 = 45 kHz of an 5 kHz vibration can be calculated. For the longer period length in case of f_2 = 43 kHz the shape of a rectangle is filled with a higher density compared to f_2 = 45 kHz; for f_2 = 45 kHz the period length of the two-dimensional vibration is shorter, thus the density of the filled rectangle shape is less.

The evaluated simulation results of the parameter sweep are the friction work and the maximum deflection of the contact point *S*. The maximum deflection can be calculated by the absolute value $\left\|\vec{l}_{W'}(t)\right\|$ of the vector from the origin P to the projection point *W*′, Fig. 5; for a one-dimensional vibration, the maximum deflection is equal to the vibration amplitude. The maximum deflection of the vibration locus is evaluated as an indicator of the mechanical stress during ultrasonic bonding; increasing the maximum deflection leads typically to higher mechanical stress for already bonded areas and therefore the risk to damage the substrate and already bonded micro junctions is increased.

The results of the parameter sweep are shown in Fig. 7; on top the ratio W_{2d}/W_{1d} between the frictional work of the multi-dimensional vibration loci and the corresponding one-dimensional vibration with the same maximum deflection as the multi-dimensional vibration is shown. The ratio is proportional to the increase of the frictional power in the interface with the multi-dimensional vibration trajectory without increasing the maximum deflection compared to the corresponding one-

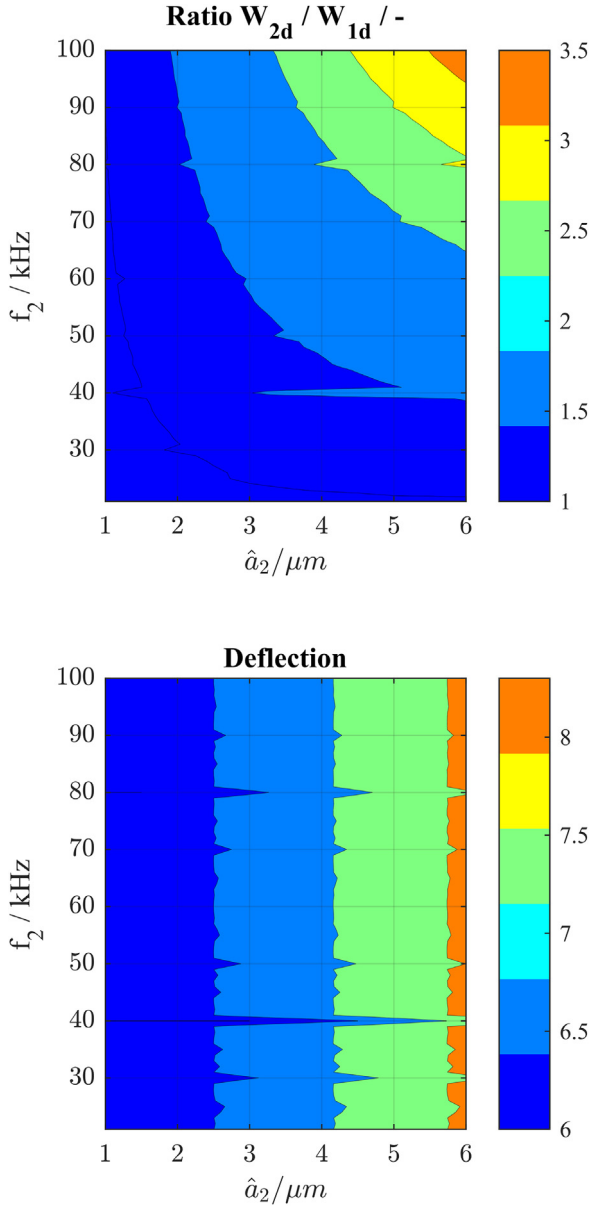

Fig. 7. Results of the parameter sweep: ratio W_{2d}/W_{1d} between the frictional work of the multi-dimensional vibration loci and the corresponding one-dimensional vibration with the same maximum deflection (top) and the maximum deflection of the multi-dimensional vibration loci (bottom).

dimensional vibration. At the bottom, the maximum deflection of the multi-dimensional vibration loci is shown. The results are plotted over the vibration amplitude $\hat{a}_2$ and the excitation frequency f_2 which are both varied in the range shown in Table 2.

By an additional vibration in y-direction with a higher frequency f_2 compared to f_1 = 20kHz, the friction work can be increased by a factor of approx. 3.5. The maximum deflection for $\hat{a}_2 = 6\ \mu m$ is about 8.5μm leading to an increase of the maximum deflection compared to the one-dimensional vibration with $\hat{a}_1 = 6\ \mu m$ of a factor about 1.4.

In general, increasing the excitation frequency f_2 for a specific excitation amplitude $\hat{a}_2$ leads to an increased frictional work in the interface; with higher excitation frequencies more oscillation cycles per time unit occur, the friction power is increased and with the constant simulation time of 4 ms, the friction work is increased.

Increasing the excitation amplitude $\hat{a}_2$ for a specific frequency leads to an increased friction work too, but also increasing the max-

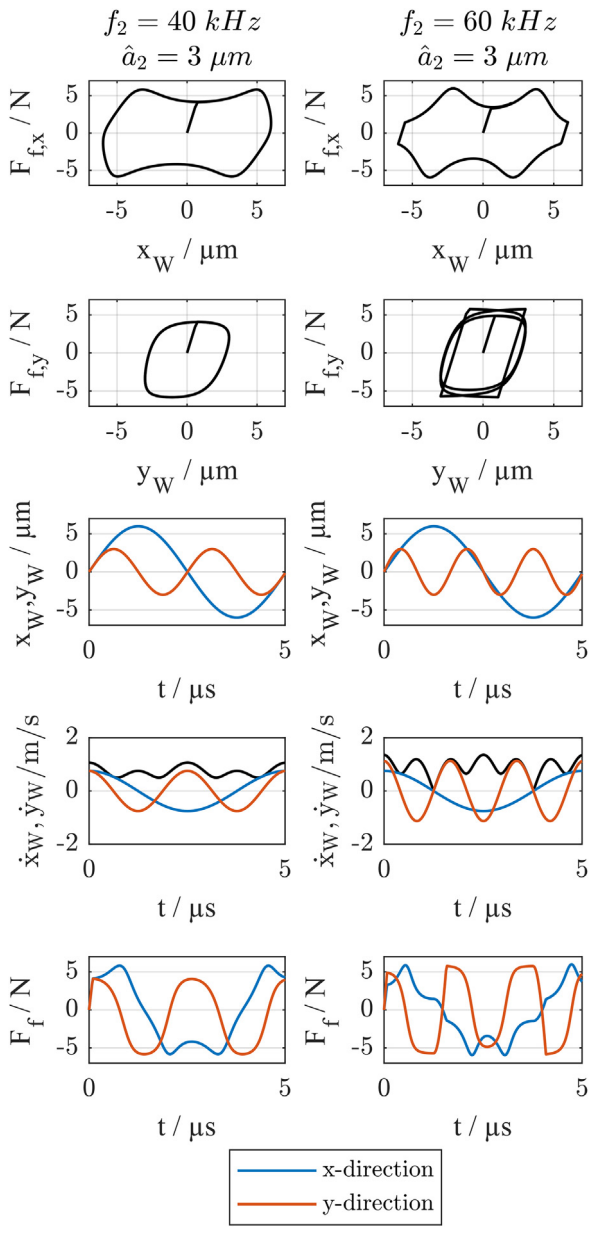

Fig. 8. From top to bottom: hystereses of friction forces in *x*- and *y*-direction, and time histories of displacement excitations x_W and y_W, the velocity excitations $\dot{x}_W$ and $\dot{y}_W$, and of the friction forces $F_{f,x}$ and $F_{f,y}$. In case of the velocities $\dot{x}_W$ and $\dot{y}_W$, also the absolute value of the two-dimensional excitation velocity is plotted as a black line. The excitation frequencies are f_1 = 20 kHz and f_2 = 40 kHz/60 kHz and the excitation amplitudes are $\hat{a}_1 = 6$ µm and $\hat{a}_2 = 3$ µm.

imum deflection which leads to higher oscillating shear forces in the substrate.

Especially for f_2 = 40 *kHz*, significantly less deflection compared to the other multi-dimensional vibration loci is reached; the reason can be seen in the form of the vibration locus shown in Fig. 6. Since the maximum amplitudes $\hat{a}_1$ and $\hat{a}_2$ never occur at the same time and because of the special ratio f_1/f_2 = 0.5 the theoretical maximum deflection $\sqrt{\hat{a}_1^2 + \hat{a}_2^2}$ is never reached.

In Fig. 8 the hystereses and the time histories of the friction forces and excitation trajectories in *x*- and *y*-direction for f_2= 40 kHz and 60 kHz are shown for the first oscillation cycle of the 20 kHz vibration x_W in *x*-direction.

For f_2 = 40 kHz the contact point S starts sliding, when the absolute value $\left\|\vec{F}_f(t)\right\|$ of the contact force reaches the sticking force value $\mu\ F_N$. Because the excitation frequency f_2 in *y*-direction is twice as high as in *x*-direction, the zero crossings of the displacement x_W in x-direction occur at the same time as the zero crossing of y_W in y-direction and when the displacement x_W reaches its maximum, y_W crosses zero again. When the displacement reaches its maximum the velocity becomes zero and the transition criterion from slip to stick Eq. (2) would be fulfilled. In case of f_2= 40 kHz, the displacement y_W in *y*-direction crosses zero again when x_W reaches its maximum, keeping the contact in the sliding regime. In general, the absolute value of the excitation velocity never reaches zero for f_2 = 40 kHz.

In contrast to the permanent sliding of the oscillation with f_2 = 40 kHz, sticking occurs with f_2 = 60 kHz. Both oscillations reach their maximum displacement amplitude at the same time in opposite direction. At this time, both excitation velocities and thus also the absolute value of the excitation velocity are zero and sticking occurs. After the first quarter of the displacement oscillation x_W, the transition from sliding to sticking occurs the first time. Sliding occurs again with the next zero crossing of the 60 kHz displacement vibration y_W and so on. The sticking phases can also be seen in the hystereses in *x*- and *y*-direction; in case of the 60 kHz hysteresis of $F_{f,y}$, the change between sticking and sliding within one period of the 20 kHz vibration can be seen.

The results of the parameter sweep show, that increasing the excitation frequency f_2 is beneficial for increasing the frictional work in the interface without increasing the mechanical stress during ultrasonic excitation. In applications with elastic contact, a minimum amplitude of the one-dimensional vibration is needed to overcome the sticking regime. For ultrasonic transducers, with rising bonding frequency, the attainable displacement amplitude of the ultrasonic transducer decreases, because the allowable velocity amplitude is approximately constant over the frequency; for titanium alloy Ti6Al4V the maximum velocity amplitude is 10 m/s and for other materials, this value is even lower, [44]. Especially for large workpieces like terminals of IGBT modules the minimum amplitudes for overcoming the sticking regime can not be reached for high bonding frequencies. In case of the multi-dimensional vibration, the smaller bonding frequency f_1 can be used to overcome the sticking regime and the second vibration with the higher bonding frequency f_2 can then be used to further increase the input power to the interface without increasing the maximum deflection as much as for the one dimensional case at the lower bonding frequency.

5. Bonding experiments

For bonding experiments the multi-dimensional transducer was operated at the resonance frequencies of approx. f_1 = 20kHz and approx. f_2 = 55kHz of the two channels and the rectangle operation mode was used. For the experiments, a new pin design for IGBT modules is used, Fig. 9. The connector pins in IGBT modules are used for switching the internal IGBTs and diodes and currently the PressFIT technology for connecting the pins with the substrate is used. A sleeve is connected with the substrate by a solder joint and afterward, the connector pin is pressed into the sleeve, [45]. For handling higher junction temperatures for future generations of the modules, a new pin design for direct ultrasonic bonds between the connector pin and the substrate was developed. At the bottom side of the new pin design a heel was added, where the ultrasonic bonding tool clamps the pin and excites a multi-dimensional vibration.

In the bonding experiments, prototypes of the new pin design made of CuSn6 and the ultrasonic bonding tool made of hardened steel with a Rockwell hardness of approx. 48 HRC were used. For the substrate direct bonded copper (DCB) was used. The design of the ultrasonic bonding tool and the pin itself are shown in

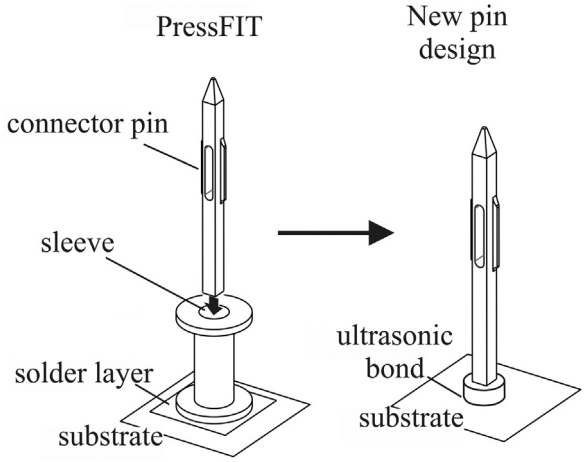

Fig. 9. Connector pin design for IGBT-modules. **Left:** PressFIT technology for joining the connector pin with the substrate. **Right:** new pin design for joining the connector pin directly with the substrate by multi-dimensional ultrasonic bonding, [45].

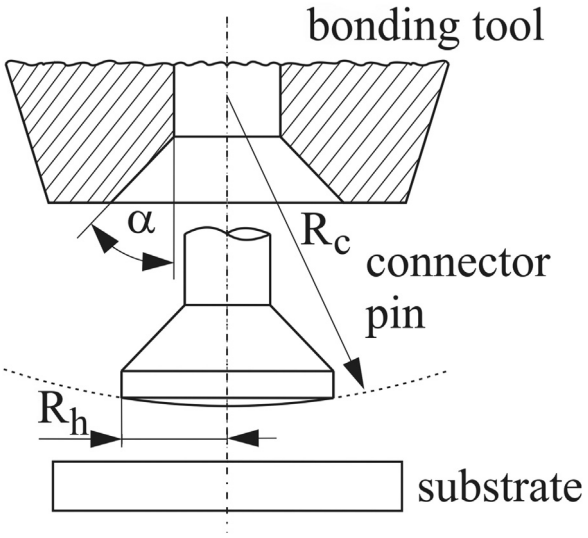

Fig. 10. Design of the bonding tool and the connector pin with an form fit clamping mechanism between the tool and pin, [41].

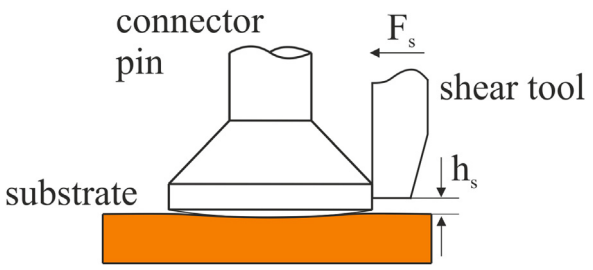

Fig. 11. Experimental setup of the shear test: the shear tool moves parallel to the substrate in direction of the connector pin in the shear height h_s. The maximum shear force value F_s during destructive testing is a measure for the bond quality.

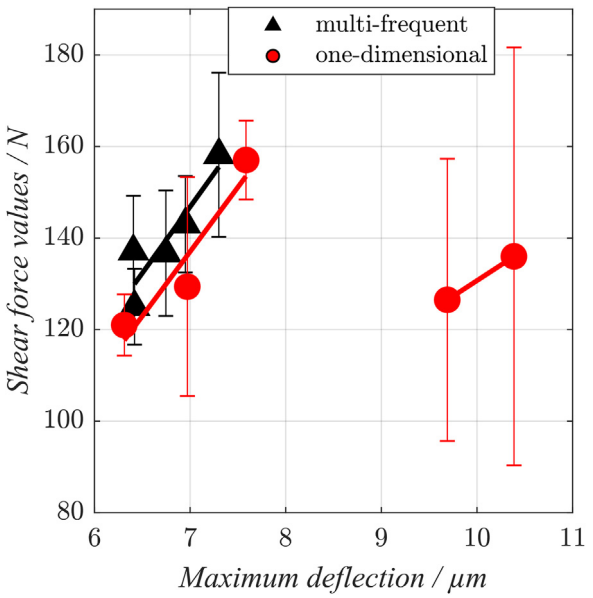

Fig. 12. Shear force values of multi-dimensional bonding experiments with the rectangle mode at the frequencies $f_1 \approx 20$kHz and $f_2 \approx 55$ kHz and one-dimensional bonding experiments at $f_1 \approx 20$ kHz. The maximum deflection is calculated from 3D laser vibrometer measurements at the tool tip by $\sqrt{\hat{a}_1^2 + \hat{a}_2^2}$ with the vibration amplitudes $\hat{a}_1$ and $\hat{a}_1$ in the two excitation directions. Both experiments were carried out with the same bond normal force and bond duration. For each parameter set, the shear force values of 10 bonds were evaluated; in the plot, mean and standard deviation values are shown.

Fig. 10. Between the bonding tool and the connector pin, form fit is achieved by the conical geometry of the clamping part of the bonding tool and the connector pin. Design parameters of the bonding tool and the connector pin are the flank angle α, the convexity radius R_c and the radius R_h at the bottom side of the connector pin. In the experiments, the design parameters $\alpha = 37.5°$, $R_c = 3$ mm and $R_h = 1$ mm were used.

For determination of the bond quality, shear force values F_s of the ultrasonically bonded pins were measured with a DAGE 4000Plus shear tester. The shear force values are determined by destructive testing by applying the shear force F_s to the connector pin parallel to the substrate in a specific height ($h_s = 25$ μm), Fig. 11. The bond connection is destroyed by the horizontal movement of the shear tool and the maximum shear force value during destructive testing is a measure for the bond quality, [46].

In the experiments, the oscillation amplitude of channel 1 with approx. 20 kHz was kept constant at 6.8 μm and the amplitude of channel 2 with approx. 55 kHz was increased up to 3 μm. For comparison between one- and two-dimensional bonding, the same multi-dimensional transducer was used, for one-dimensional bonding experiments at approx. 20 kHz; for this, the amplitude of channel 2 was set to zero and the amplitude of channel 1 was increased beginning from approx. 6.8 μm.

Both experiments were carried out with the same bond normal force (60 N) and bond duration (400 ms). The vibration amplitude was measured with a 3D laser vibrometer at the tool tip for all bonds and the mean value over the bond duration is evaluated. The results of the bonding experiments are shown in Fig. 12. With rising amplitude $\hat{a}_2$ for the multi-dimensional bonding experiments, the shear values increase from approx. 120 N for $\hat{a}_2 = 0$ μm to approx. 160 N for $\hat{a}_2 = 3$ μm.

In case of the one-dimensional bonding experiments, the shear force values also increase to approx. 160 N at an oscillation amplitude $\hat{a}_1 = 7.6$ μm. Further increasing the input power leads to an abrupt drop of the shear force values and increases the vibration amplitude of the tool significantly. The reason was found in the increased input power and higher oscillation amplitude; already bonded areas were destroyed because of high oscillating shear stress. This leads to decreasing shear force values and less damping of the vibrating tool with higher oscillation amplitudes. Also, compared to the one-dimensional ultrasonic bonding process, with the rectangle mode the shear force values are reached at slightly lower

maximum deflection, compared to the one-dimensional process for a maximum deflection <8 μm.

During the bond formation, highspeed camera videos with 20000 fps were recorded; it was found that no rotation of the connector pin occurred as has been reported in [41]. The reason can be seen in the missing circular ultrasonic excitation of the connector pin; the excitation with constantly changing orientation leads to a stable position of the rotationally symmetric pin and thus to a more robust bond process.

6. Summary and Outlook

In this contribution, the concept of an versatile multi-dimensional transducer and the control concept for two different operation modes is presented. The first operation mode is used for planar circular vibration loci ("circular mode") and with the presented control concept, the variation of the amplitude ratio between the two vibration directions is possible. The second operation mode ("rectangle mode") is used for multi-frequent planar vibration loci. Both operation modes have been validated under loaded conditions during ultrasonic bonding by 3D laser vibrometer measurements at the tool-tip.

In simulations with a two-dimensional friction model, the impact of different multi-frequent vibration loci was investigated. Depending on the ratio between the two excitation frequencies, the frictional power in the interface can be increased significantly. Additionally, the maximum deflection of the multi-dimensional vibration is less compared to a one-dimensional vibration with the same frictional power, meaning that the oscillating mechanical shear stress in the substrate is less for a multi-dimensional vibration.

In ultrasonic bonding experiments with a new connector pin design for IGBT-modules, the multi-frequent rectangle mode with the two bonding frequencies $f_1 \approx 20$ kHz and $f_2 \approx 55$ kHz was compared to a one-dimensional ultrasonic bonding process with the bonding frequency $f_1 \approx 20$kHz. It was found, that the same shear force values with the rectangle mode could be reached compared to the one-dimensional bond process, but with slightly lower maximum deflection. In case of the one-dimensional bonding experiments and the tested range for the vibration amplitudes, the shear force values dropped when the vibration amplitude was increased beyond 8 μm. These results indicate, that for the multi-dimensional ultrasonic bonding a wider process window in terms of higher ultrasonic power can be achieved compared to one-dimensional bonding.

The findings of this contribution provide a profound understanding of the principles of multi-dimensional and multi-frequent ultrasonic bonding for future investigations. These should include

- analysis of cross-section images of the interface for one- and two-dimensional bonding. This provides further information on the effect of multi-dimensional bonding on the mechanical stress to the interface by evaluating the changes of the micro-structure of the metals, the deformation of the substrate and failure modes like cracks in the substrate material.
- further experiments with a larger process parameter window to evaluate if multi-dimensional bonding with higher ultrasonic power compared to one-dimensional bonding is possible to further increase the shear force values without damaging the substrate.

Acknowledgements

This research was supported by ERDF.NRW (European Regional Development Fund in North Rhine-Westphalia).

References

[1] A. Weston, Wire bonding as a technique for semiconductor device assembly, Microelectron. Int. 2 (3) (1985) 26–35, http://dx.doi.org/10.1108/eb044183.
[2] Y. Long, J. Twiefel, J. Wallaschek, A review on the mechanisms of ultrasonic wedge-wedge bonding, J. Mater. Process. Technol. 245 (2017) 241–258.
[3] R. Schemmel, T. Hemsel, W. Sextro, Numerical and experimental investigations in ultrasonic heavy wire bonding, 6th European Conference on Computational Mechanics (ECCM 6) (2018).
[4] A. Unger, W. Sextro, S. Althoff, P. Eichwald, T. Meyer, F. Eacock, M. Brökelmann, M. Hunstig, D. Bolowski, K. Guth, Experimental and numerical simulation study of pre-deformed heavy copper wire wedge bonds, in: in: Proceedings of the 47th International Symposium on Microelectronics (IMAPS), San Diego, CA, US, 2014, pp. 289–294.
[5] Y. Long, F. Dencker, A. Isaak, J. Hermsdorf, M. Wurz, J. Twiefel, Self-cleaning mechanisms in ultrasonic bonding of al wire, J. Mater. Process. Technol. 258 (2018) 58–66.
[6] Y. Long, F. Dencker, A. Isaak, C. Li, F. Schneider, J. Hermsdorf, M. Wurz, J. Twiefel, J. Wallaschek, Revealing of ultrasonic wire bonding mechanisms via metal-glass bonding, Mater. Sci. Eng.: B (2018), http://dx.doi.org/10.1016/j.mseb.2018.11.010.
[7] Y. Daud, M. Lucas, Z. Huang, Modelling the effects of superimposed ultrasonic vibrations on tension and compression tests of aluminium, J. Mater. Process. Technol. 186 (1) (2007) 179–190, http://dx.doi.org/10.1016/j.jmatprotec.2006.12.032.
[8] K.B. Pedersen, D. Benning, P.K. Kristensen, V.N. Popok, K. Pedersen, Interface structure and strength of ultrasonically wedge bonded heavy aluminium wires in si-based power modules, J. Mater. Sci.: Mater. Electron. 25 (7) (2014) 2863–2871, http://dx.doi.org/10.1007/s10854-014-1953-8.
[9] D. Tabor, Junction growth in metallic friction: the role of combined stresses and surface contamination, Proc. Royal Soc. London A: Math. Phys. Eng. Sciences 251 (1266) (1959) 378–393, http://dx.doi.org/10.1098/rspa.1959.0114.
[10] M. Sbeiti, Thermomechanische beschreibung der ausbildung einer intermetallischen phase beim ultraschall-wedge/wedge-drahtbonden im rahmen der theorie der materiellen kräfte, Ph.D. thesis, 2013.
[11] Y. Ding, J.-K. Kim, Numerical analysis of ultrasonic wire bonding: Part 2. effects of bonding parameters on temperature rise, Microelectron. Reliability 48 (1) (2008) 149–157, http://dx.doi.org/10.1016/j.microrel.2007.01.083.
[12] Y.Y. Zhao, D. Li, Y.S. Zhang, Effect of welding energy on interface zone of al-cu ultrasonic welded joint, Sci. Technol. Weld. Join. 18 (4) (2013) 354–360, http://dx.doi.org/10.1179/1362171813Y.0000000114.
[13] A. Das, I. Masters, D. Williams, Process robustness and strength analysis of multi-layered dissimilar joints using ultrasonic metal welding, Int. J. Adv. Manuf. Technol. (Nov 2018), http://dx.doi.org/10.1007/s00170-018-2936-3.
[14] P. Chauhan, Z.W. Zhong, M. Pecht, Copper wire bonding concerns and best practices, J. Electron. Mater. 42 (8) (2013) 2415–2434, http://dx.doi.org/10.1007/s11664-013-2576-1.
[15] D. Kim, R. Willmot, D. Peroulis, A high-efficiency low-cost wire-bond loop antenna for cmos wafers, 2009 IEEE Antennas and Propagation Society International Symposium (2009) 1–4.
[16] R. Gilardoni, Ribbon bonding for high frequency applications advantages of ribbon and the impact on the microwave market, in: IMAPS/SEMI Advanced technology workshop on wire bonding, San Francisco (2008) 1–5.
[17] B. Ong, M. Helmy, S. Chuah, C. Luechinger, G. Wong, Heavy al ribbon interconnect: An alternative solution for hybrid power packaging, in: Proc, 37th Int. Symposium on Microelectronics, IMAPS (2004).
[18] N. Marenco, M. Kontek, W. Reinert, J. Lingner, M. Poech, Copper ribbon bonding for power electronics applications, in: 2013 Eurpoean Microelectronics Packaging Conference (EMPC) (2013) 1–4.
[19] S. Mostafavi, D.F. Hesser, B. Markert, Effect of process parameters on the interface temperature in ultrasonic aluminum wire bonding, J. Manuf. Process. 36 (2018) 104–114, http://dx.doi.org/10.1016/j.jmapro.2018.09.020.
[20] Y. Nishimura, K. Kido, F. Momose, T. Goto, Development of ultrasonic welding for igbt module structure, in: 2010 22nd International Symposium on Power Semiconductor Devices IC's (ISPSD) (2010) 293–296.
[21] S. Nambu, K. Seto, J.-Y. Lin, T. Koseki, Development of a bonding interface between steel/steel and steel/ni by ultrasonic welding, Sci. Technol. Weld. Join. 23 (8) (2018) 687–692, http://dx.doi.org/10.1080/13621718.2018.1473077.
[22] B. Sanga, R. Wattal, D.S. Nagesh, Mechanism of joint formation and characteristics of interface in ultrasonic welding: Literature review, Period. Eng. Nat. Sci. (PEN) 6 (2018) 107, http://dx.doi.org/10.21533/pen.v6i1.158.
[23] R. John, O. Vermesan, R. Bayerer, High temperature power electronics igbt modules for electrical and hybrid vehicles, IMAPS, High Temperature Electronics Network (HiTEN) 1 (2009) 199–204.
[24] A. Karch, Neue lötlegierung für erweiterte einsatztemperaturen, 2018.
[25] V. Müller, H. Lewitschnig, N. Kortik, W. Kanert, Quality assurance in automotive electronics, Elektrotechnik und Informationstechnik 128 (2011) 371–374, http://dx.doi.org/10.1007/s00502-011-0048-y.
[26] L. Levine, The ultrasonic wedge bonding mechanism: Two theories converge, ISHM 95 (1995) 242–246.
[27] J. Onuki, M. Koizumi, I. Ishikawa, Effects of frequency and surface cleanliness of al–si electrode on ultrasonic bonding characteristics of thick al wire bonding, Mater. Trans. JIM 37 (9) (1996) 1492–1496, http://dx.doi.org/10.2320/matertrans1989.37.1492.

[28] Y.H. Chan, J.-K. Kim, D. Liu, P.C.K. Liu, Y.M. Cheung, M.W. Ng, Effects of bonding frequency on au wedge wire bondability, J. Mater. Sci.: Mater. Electron. 19 (3) (2008) 281–288, http://dx.doi.org/10.1007/s10854-007-9312-7.
[29] H.K. Charles, K.J. Mach, S.J. Lehtonen, A.S. Francomacaro, J.S. DeBoy, R.L. Edwards, High-frequency wirebonding: process and reliability implications, in: 52nd Electronic Components and Technology Conference 2002. (Cat. No.02CH37345) (2002) 881–890, http://dx.doi.org/10.1109/ECTC.2002.1008204.
[30] H. Charles, K. Mach, S. Lehtonen, A. Francomacaro, J. DeBoy, R. Edwards, Wirebonding at higher ultrasonic frequencies: reliability and process implications, Microelectron. Reliability 43 (1) (2003) 141–153, http://dx.doi.org/10.1016/S0026-2714(02)00118-X.
[31] G. Heinen, R.J. Stierman, D. Edwards, L. Nye, Wire bonds over active circuits, in: 1994 Proceedings, 44th Electronic Components and Technology Conference (1994) 922–928, http://dx.doi.org/10.1109/ECTC.1994.367518.
[32] R. Schemmel, S. Althoff, W. Sextro, A. Unger, M. Hunstig, M. Broekelmann, Effects of different working frequencies on the joint formation in copper wire bonding, in: CIPS 2018; 10th International Conference on Integrated Power Electronics Systems (2018) 1–6, URL http://ieeexplore.ieee.org/stamp/stamp.jsp?tp=&arnumber=8403137&isnumber=8402818.
[33] J. Tsujino, T. Tamura, T. Uchida, T. Ueoka, Characteristics of two-vibration-system ultrasonic plastic welding with 90 khz and 20 khz vibration systems at right angles, Jpn. J. Appl. Phys. 35 (11R) (1996) 5884.
[34] T. Asami, Y. Higuchi, H. Miura, Ultrasonic metal welding by longitudinal-torsional vibration source consisting of two transducers, J. Acoust. Soc. Am. 140 (4) (2016) 3423, http://dx.doi.org/10.1121/1.4971013.
[35] E. Hetrick, J. Baer, W. Zhu, L. Reatherford, A. Grima, D. Scholl, D. Wilkosz, S. Fatima, S. Ward, Ultrasonic metal welding process robustness in aluminum automotive body construction applications, Weld. J. 88 (7) (2009) 149–158.
[36] T. Asami, H. Miura, Ultrasonic welding of dissimilar metals by vibration with planar locus, Acoustical Sci. Technol. 36 (3) (2015) 232–239, http://dx.doi.org/10.1250/ast.36.232.
[37] T. Asami, H. Miura, Longitudinal-torsional vibration source consisting of two transducers with different vibration modes, Jpn. J. Appl. Phys. 55 (7S1) (2016) 07KE08.
[38] T. Asami, Y. Tamada, Y. Higuchi, H. Miura, Ultrasonic metal welding with a vibration source using longitudinal and torsional vibration transducers, Jpn. J. Appl. Phys. 56 (7S1) (2017) 07JE02.
[39] Y. Tamada, T. Asami, H. Miura, Welding characteristics of cu and al plates using planar vibration by a dumbbell-shaped ultrasonic complex vibration source, Jpn. J. Appl. Phys. 57 (7S1) (2018) 07LE12.
[40] C. Dymel, R. Schemmel, T. Hemsel, W. Sextro, M. Brökelmann, M. Hunstig, Experimental investigations on the impact of bond process parameters in two-dimensional ultrasonic copper bonding, in: in: Proceedings of IEEE CPMT Symposium Japan, Kyoto, Japan, 2018, 2018, pp. 1–4.
[41] C. Dymel, P. Eichwald, R. Schemmel, T. Hemsel, M. Brökelmann, M. Hunstig, W. Sextro, Numerical and statistical investigation of weld formation in a novel two-dimensional copper-copper bonding process, in: in: (Proceedings of 7th Electronics System-Integration Technology Conference, Dresden, Germany), 2018, pp. 1–6.
[42] B. Yang, C. Menq, Characterization of 3d contact kinematics and prediction of resonant response of structures having 3d frictional constraint, J. Sound Vibr. 217 (5) (1998) 909–925, http://dx.doi.org/10.1006/jsvi.1998.1802.
[43] L. Panning, Auslegung von Reibelementen zur Schwingungsdämpfung von Turbinenschaufeln, Fortschritt-Berichte VDI: Reihe 11, Schwingungstechnik, VDI-Verlag, 2005 https://books.google.de/books?id=OVHAAgAACAAJ.
[44] E.-G. Lierke, W. Littmann, T. Hemsel, Zur theorie der piezoelektrischen ultraschallverbundschwinger mit praktischen schlussfolgerungen für den entwicklungsingenieur, 2010 http://digital.ub.uni-paderborn.de/ubpb/urn/urn:nbn:de:hbz:466:2-7370.
[45] P. Eichwald, S. Althoff, R. Schemmel, W. Sextro, A. Unger, M. Brökelmann, M. Hunstig, Multi-dimensional ultrasonic copper bonding - new challenges for tool design, IMAPSource 2017 (1) (2017), http://dx.doi.org/10.4071/isom-2017-WP43_071.
[46] German Welding Society (DVS), Technical Bulletin DVS 2811 - Test Procedures for Wire Bonded Joints, Tech. rep., Translation of the German issue, 2017.

Biographies

Reinhard Schemmel studied Mechanical Engineering at Paderborn University and graduated with distinction at the end of 2016. Since then he is a research assistant at the Chair for Dynamics and Mechatronics at Paderborn University. His research interests focus on ultrasonic bonding, sensors, and actuators, especially piezoelectric systems.

Tobias Hemsel studied Mechanical Engineering at Paderborn University. After graduating in 1996 he was a research assistant at the Heinz Nixdorf Institute and received his PhD in 2001. Since then he is engineering head at the Chair for Dynamics and Mechatronics at Paderborn University. His research interests focus on sensors and actuators, especially piezoelectric systems.

Collin Dymel studied Mechanical Engineering at University of Duisburg-Essen. After graduating in 2013, he designed and developed compact and lightweight electro-hydraulic actuators and piezo-pneumatic valves for Hoerbiger Automatisierungstechnik GmbH, Stuttgart, Germany. In 2017, he joined the Chair for Dynamics and Mechatronics at Paderborn University. His research interests focus on ultrasonic bonding, sensors and actuators with the focus on piezoelectric systems.

Matthias Hunstig studied mechanical engineering at Paderborn University, Germany. From 2008 to 2013, he worked as a research assistant at Paderborn University. Since 2013, he has been working for Hesse GmbH, a leading supplier of ultrasonic wire bonding machines for the semiconductor industry, where he is currently deputy head of research, working on ultrasonic bonding systems and new interconnection technologies. He received a doctorate from Paderborn University in 2014 for his work on fast piezoelectric inertia motors.

Michael Brökelmann studied mechanical engineering at Paderborn University and the University of Waterloo Canada and received a doctorate in 2008 for his work on process integrated quality control in ultrasonic wire bonding. Since 2006 he is working as a senior engineer at Hesse GmbH, a leading manufacturer of ultrasonic wire bonding machines. He mainly works on the design and evaluation of ultrasonic systems, bond process analysis and on new developments in interconnection technology. Since 2016 he is heading the research department at Hesse GmbH.

Walter Sextro studied Mechanical Engineering at the Leibnitz University Hanover and Imperial College in London. After graduating, he designed and optimized drill strings for Baker Hughes Inteq research in Celle, Germany and Houston, Texas. He received his PhD from the Leibnitz University Hanover in 1997. Subsequently, he qualified as a professor in the field of mechanics and published his habilitation thesis. In 2004 he was appointed as a professor at the institute of mechanics and gear trains at the Technical University of Graz, Austria. Since 2009 he leads the Chair for Dynamics and Mechatronics at Paderborn University.